

<sup>1</sup> Geometric models reveal behavioral and neural  
<sup>2</sup> signatures of transforming naturalistic experiences into  
<sup>3</sup> episodic memories

<sup>4</sup> Andrew C. Heusser<sup>1, 2, †</sup>, Paxton C. Fitzpatrick<sup>1, †</sup>, and Jeremy R. Manning<sup>1, \*</sup>

<sup>1</sup>Department of Psychological and Brain Sciences

Dartmouth College, Hanover, NH 03755, USA

<sup>2</sup>Akili Interactive

Boston, MA 02110

<sup>†</sup>Denotes equal contribution

<sup>\*</sup>Corresponding author: Jeremy.R.Manning@Dartmouth.edu

<sup>5</sup> September 3, 2020

## Abstract

The mental contexts in which we interpret experiences are often person-specific, even when the experiences themselves are shared. We developed a geometric framework for mathematically characterizing the subjective conceptual content of dynamic naturalistic experiences. We model experiences and memories as *trajectories* through word embedding spaces whose coordinates reflect the universe of thoughts under consideration. Memory encoding can then be modeled as geometrically preserving or distorting the *shape* of the original experience. We applied our approach to data collected as participants watched and verbally recounted a television episode while undergoing functional neuroimaging. Participants' recounts all preserved coarse spatial properties (essential narrative elements), but not fine spatial scale (low-level) details, of the episode's trajectory. We also identified networks of brain structures sensitive to these trajectory shapes. Our work provides insights into how our brains preserve and distort our ongoing experiences when we encode them into episodic memories.

## Introduction

What does it mean to *remember* something? In traditional episodic memory experiments (e.g., list-learning or trial-based experiments; Kahana, 1996; Murdock, 1962), remembering is often cast as a discrete binary operation: each studied item may be separated from the rest of one's experience and labeled as having been either recalled or forgotten. More nuanced studies might incorporate self-reported confidence measures as a proxy for memory strength, or ask participants to discriminate between recollecting the (contextual) details of an experience and having a general feeling of familiarity (Yonelinas, 2002). Using well-controlled, trial-based experimental designs, the field has amassed a wealth of information regarding human episodic memory (for review see Kahana, 2012). However, there are fundamental properties of the external world and our memories that trial-based experiments are not well suited to capture (for review, also see Huk et al., 2018; Koriat and Goldsmith, 1994). First, our experiences and memories are continuous, rather than discrete—isolating a naturalistic event from the context in which it occurs can substantially change its meaning. Second, whether or not the rememberer has precisely reproduced a specific set of words

33 in describing a given experience is nearly orthogonal to how well they were actually able to  
34 remember it. In classic (e.g., list-learning) memory studies, by contrast, the number or proportion  
35 of *exact* recalls is often considered to be a primary metric for assessing the quality of participants'  
36 memories. Third, one might remember the essence (or a general summary) of an experience but  
37 forget (or neglect to recount) particular low-level details. Capturing the essence of what happened  
38 is often a main goal of recounting an episodic memory to a listener, whereas the inclusion of specific  
39 low-level details is often less pertinent.

40 How might we formally characterize the *essence* of an experience, and whether it has been  
41 recovered by the rememberer? And how might we distinguish an experience's overarching essence  
42 from its low-level details? One approach is to start by considering some fundamental properties  
43 of the dynamics of our experiences. Each given moment of an experience tends to derive meaning  
44 from surrounding moments, as well as from longer-range temporal associations (Lerner et al., 2011;  
45 Manning, 2019, 2020). Therefore, the timecourse describing how an event unfolds is fundamental  
46 to its overall meaning. Further, this hierarchy formed by our subjective experiences at different  
47 timescales defines a *context* for each new moment (e.g., Howard and Kahana, 2002; Howard  
48 et al., 2014), and plays an important role in how we interpret that moment and remember it  
49 later (for review see Manning, 2020; Manning et al., 2015). Our memory systems can leverage  
50 these associations to form predictions that help guide our behaviors (Ranganath and Ritchey,  
51 2012). For example, as we navigate the world, the features of our subjective experiences tend  
52 to change gradually (e.g., the room or situation we find ourselves in at any given moment is  
53 strongly temporally autocorrelated), allowing us to form stable estimates of our current situation  
54 and behave accordingly (Zacks et al., 2007; Zwaan and Radvansky, 1998).

55 Occasionally, this gradual drift of our ongoing experience is punctuated by sudden changes,  
56 or shifts (e.g., when we walk through a doorway; Radvansky and Zacks, 2017). Prior research  
57 suggests that these sharp transitions (termed *event boundaries*) help to discretize our experiences  
58 (and their mental representations) into *events* (Brunec et al., 2018; Clewett and Davachi, 2017;  
59 DuBrow and Davachi, 2013; Ezzyat and Davachi, 2011; Heusser et al., 2018a; Radvansky and  
60 Zacks, 2017). The interplay between the stable (within-event) and transient (across-event) temporal

61 dynamics of an experience also provides a potential framework for transforming experiences  
62 into memories that distills those experiences down to their essences. For example, prior work  
63 has shown that event boundaries can influence how we learn sequences of items (DuBrow and  
64 Davachi, 2013; Heusser et al., 2018a), navigate (Brunec et al., 2018), and remember and understand  
65 narratives (Ezzyat and Davachi, 2011; Zwaan and Radvansky, 1998). This work also suggests  
66 a means of distinguishing the essence of an experience from its low-level details. The overall  
67 structure of events and event transitions reflects how the high-level experience unfolds (i.e., its  
68 essence), while subtler event-level properties reflect low-level details. Prior research has also  
69 implicated a network of brain regions (including the hippocampus and the medial prefrontal  
70 cortex) in playing a critical role in transforming experiences into structured and consolidated  
71 memories (Tompry and Davachi, 2017).

72 Here, we sought to examine how the temporal dynamics of a naturalistic experience were later  
73 reflected in participants' memories. We also sought to leverage the above conceptual insights into  
74 the distinctions between an experience's essence and its low-level details to build models that  
75 explicitly quantified these distinctions. We analyzed an open dataset that comprised behavioral  
76 and functional Magnetic Resonance Imaging (fMRI) data collected as participants viewed and then  
77 verbally recounted an episode of the BBC television show *Sherlock* (Chen et al., 2017). We developed  
78 a computational framework for characterizing the temporal dynamics of the moment-by-moment  
79 content of the episode, and of participants' verbal recalls. Our framework uses topic modeling (Blei  
80 et al., 2003) to characterize the thematic conceptual (semantic) content present in each moment of the  
81 episode and recalls by projecting each moment into a word embedding space. We then use hidden  
82 Markov models (Baldassano et al., 2017; Rabiner, 1989) to discretize this evolving semantic content  
83 into events. In this way, we cast both naturalistic experiences and memories of those experiences  
84 as geometric *trajectories* through word embedding space that describe how they evolve over time.  
85 Under this framework, successful remembering entails verbally traversing the content trajectory  
86 of the episode, thereby reproducing the shape (essence) of the original experience. Our framework  
87 captures the episode's essence in the sequence of geometric coordinates for its events, and its  
88 low-level details by examining its within-event geometric properties.

89 Comparing the overall shapes of the topic trajectories for the episode and participants' recalls  
90 reveals which aspects of the episode's essence were preserved (or discarded) in the translation into  
91 memory. We also develop two metrics for assessing participants' memories for low-level details:  
92 (1) the *precision* with which a participant recounts details about each event, and (2) the *distinctiveness*  
93 of each recalled event, relative to other events. We examine how these metrics relate to overall  
94 memory performance as judged by third-party human annotators. We also compare and contrast  
95 our general approach to studying memory for naturalistic experiences with standard metrics for  
96 assessing performance on more traditional memory tasks, such as list-learning. Last, we leverage  
97 our framework to identify networks of brain structures whose responses (as participants watched  
98 the episode) reflected the temporal dynamics of the episode and/or how participants would later  
99 recount it.

## 100 Results

101 To characterize the dynamic content of the *Sherlock* episode and participants' subsequent recounts  
102ings, we used a topic model (Blei et al., 2003) to discover the episode's latent themes. Topic models  
103 take as inputs a vocabulary of words to consider and a collection of text documents, and return  
104 two output matrices. The first of these is a *topics matrix* whose rows are *topics* (or latent themes)  
105 and whose columns correspond to words in the vocabulary. The entries in the topics matrix  
106 reflect how each word in the vocabulary is weighted by each discovered topic. For example, a  
107 detective-themed topic might weight heavily on words like "crime," and "search." The second  
108 output is a *topic proportions matrix*, with one row per document and one column per topic. The  
109 topic proportions matrix describes the mixture of discovered topics reflected in each document.

110 Chen et al. (2017) collected hand-annotated information about each of 1,000 (manually identi-  
111 fied) scenes spanning the roughly 50 minute video used in their study. This information included:  
112 a brief narrative description of what was happening, the location where the scene took place, the  
113 names of any characters on the screen, and other similar details (for a full list of annotated fea-  
114 tures, see *Methods*). We took from these annotations the union of all unique words (excluding stop

words, such as “and,” “or,” “but,” etc.) across all features and scenes as the vocabulary for the topic model. We then concatenated the sets of words across all features contained in overlapping sliding windows of (up to) 50 scenes, and treated each window as a single document for the purpose of fitting the topic model. Next, we fit a topic model with (up to)  $K = 100$  topics to this collection of documents. We found that 32 unique topics (with non-zero weights) were sufficient to describe the time-varying content of the episode (see *Methods*; Figs. 1, S2). We note that our approach is similar in some respects to Dynamic Topic Models (Blei and Lafferty, 2006), in that we sought to characterize how the thematic content of the episode evolved over time. However, whereas Dynamic Topic Models are designed to characterize how the properties of *collections* of documents change over time, our sliding window approach allows us to examine the topic dynamics within a single document (or video). Specifically, our approach yielded (via the topic proportions matrix) a single *topic vector* for each sliding window of annotations transformed by the topic model. We then stretched (interpolated) the resulting windows-by-topics matrix to match the time series of the 1,976 fMRI volumes collected as participants viewed the episode.

The 32 topics we found were heavily character-focused (i.e., the top-weighted word in each topic was nearly always a character) and could be roughly divided into themes centered around Sherlock Holmes (the titular character), John Watson (Sherlock’s close confidant and assistant), supporting characters (e.g., Inspector Lestrade, Sergeant Donovan, or Sherlock’s brother Mycroft), or the interactions between various groupings of these characters (see Fig. S2). This likely follows from the frequency with which these terms appeared in the episode annotations. Several of the identified topics were highly similar, which we hypothesized might allow us to distinguish between subtle narrative differences if the distinctions between those overlapping topics were meaningful. The topic vectors for each timepoint were also *sparse*, in that only a small number (typically one or two) of topics tended to be “active” in any given timepoint (see Fig. 2A). Further, the dynamics of the topic activations appeared to exhibit *persistence* (i.e., given that a topic was active in one timepoint, it was likely to be active in the following timepoint) along with *occasional rapid changes* (i.e., occasionally topic weights would change abruptly from one timepoint to the next). These two properties of the topic dynamics may be seen in the block diagonal structure of the timepoint-by-

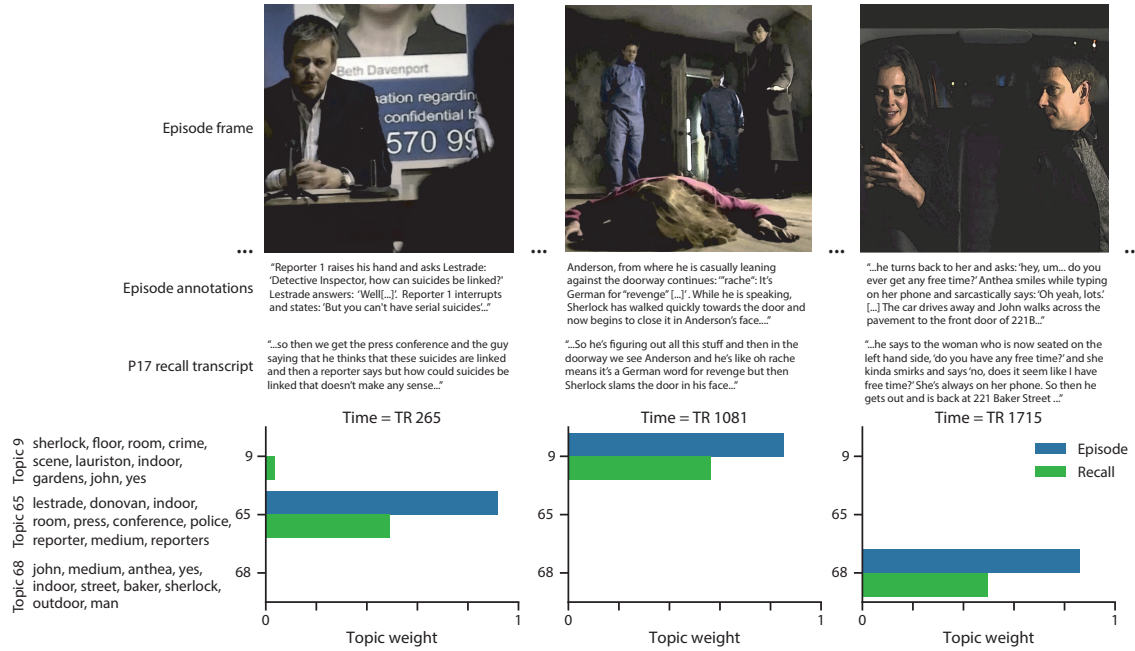


**Figure 1: Topic weights in episode and recall content.** We used hand-annotated descriptions of each manually identified scene from the episode to fit a topic model. Three example episode frames (first row) and their associated descriptions (second row) are displayed. The third row shows an example participant’s recounts of the same three scenes. We used the topic model (fit to the episode annotations) to estimate topic vectors for each moment of the episode and each sentence of participants’ recalls. Example topic vectors are displayed in the bottom row (blue: episode annotations; green: example participant’s recalls). Three topic dimensions are shown (the highest-weighted topics for each of the three example scenes, respectively), along with the 10 highest-weighted words for each topic. Figure S2 provides a full list of the top 10 words from each of the discovered topics.

143 timepoint correlation matrix (Fig. 2B) and reflect the gradual drift and sudden shifts fundamental  
144 to the temporal dynamics of many real-world experiences, as well as television episodes. Given  
145 this observation, we adapted an approach devised by Baldassano et al. (2017), and used a hidden  
146 Markov model (HMM) to identify the *event boundaries* where the topic activations changed rapidly  
147 (i.e., the boundaries of the blocks in the temporal correlation matrix; event boundaries identified  
148 by the HMM are outlined in yellow in Fig. 2B). Part of our model fitting procedure required  
149 selecting an appropriate number of events into which the topic trajectory should be segmented.  
150 To accomplish this, we used an optimization procedure that maximized the difference between the  
151 topic weights for timepoints within an event versus timepoints across multiple events (see *Methods*  
152 for additional details). We then created a stable summary of the content within each episode event  
153 by averaging the topic vectors across the timepoints spanned by each event (Fig. 2C).

154 Given that the time-varying content of the episode could be segmented cleanly into discrete  
155 events, we wondered whether participants' recalls of the episode also displayed a similar structure.  
156 We applied the same topic model (already trained on the episode annotations) to each participant's  
157 recalls. Analogously to how we parsed the time-varying content of the episode, to obtain similar  
158 estimates for each participant's recall transcript, we treated each overlapping window of (up to)  
159 10 sentences from their transcript as a document, and computed the most probable mix of topics  
160 reflected in each timepoint's sentences. This yielded, for each participant, a number-of-windows  
161 by number-of-topics topic proportions matrix that characterized how the topics identified in the  
162 original episode were reflected in the participant's recalls. An important feature of our approach  
163 is that it allows us to compare participants' recalls to events from the original episode, despite  
164 that different participants used widely varying language to describe the events, and that those  
165 descriptions often diverged in content and quality from the episode annotations. This ability  
166 to match up conceptually related text that differs in specific vocabulary, detail, and length is an  
167 important benefit of projecting the episode and recalls into a shared topic space. An example topic  
168 proportions matrix from one participant's recalls is shown in Figure 2D.

169 Although the example participant's recall topic proportions matrix has some visual similarity  
170 to the episode topic proportions matrix, the time-varying topic proportions for the example par-



**Figure 2: Modeling naturalistic stimuli and recalls.** All panels: darker colors indicate greater values; range: [0, 1]. **A.** Topic vectors ( $K = 100$ ) for each of the 1976 episode timepoints. **B.** Timepoint-by-timepoint correlation matrix of the topic vectors displayed in Panel A. Event boundaries discovered by the HMM are denoted in yellow (30 events detected). **C.** Average topic vectors for each of the 30 episode events. **D.** Topic vectors for each of 265 sliding windows of sentences spoken by an example participant while recalling the episode. **E.** Timepoint-by-timepoint correlation matrix of the topic vectors displayed in Panel D. Event boundaries detected by the HMM are denoted in yellow (22 events detected). For similar plots for all participants, see Figure S4. **F.** Average topic vectors for each of the 22 recall events from the example participant. **G.** Correlations between the topic vectors for every pair of episode events (Panel C) and recall events (from the example participant; Panel F). For similar plots for all participants, see Figure S5. **H.** Average correlations between each pair of episode events and recall events (across all 17 participants). To create the figure, each recalled event was assigned to the episode event with the most correlated topic vector (yellow boxes in panels G and H).

ticipant's recalls are not as sparse as those for the episode (compare Figs. 2A and D). Similarly, although there do appear to be periods of stability in the recall topic dynamics (i.e., most topics are active or inactive over contiguous blocks of time), the changes in topic activations that define event boundaries appear less clearly delineated in participants' recalls than in the episode's annotations. To examine these patterns in detail, we computed the timepoint-by-timepoint correlation matrix for the example participant's recall topic proportions matrix (Fig. 2E). As in the episode correlation matrix (Fig. 2B), the example participant's recall correlation matrix has a strong block diagonal structure, indicating that their recalls are discretized into separated events. We used the same HMM-based optimization procedure that we had applied to the episode's topic proportions matrix (see *Methods*) to estimate an analogous set of event boundaries in the participant's recounting of the episode (outlined in yellow). We carried out this analysis on all 17 participants' recall topic proportions matrices (Fig. S4).

Two clear patterns emerged from this set of analyses. First, although every individual participant's recalls could be segmented into discrete events (i.e., every individual participant's recall correlation matrix exhibited clear block diagonal structure; Fig. S4), each participant appeared to have a unique *recall resolution*, reflected in the sizes of those blocks. While some participants' recall topic proportions segmented into just a few events (e.g., Participants P4, P5, and P7), others' segmented into many shorter duration events (e.g., Participants P12, P13, and P17). This suggests that different participants may be recalling the episode with different levels of detail—i.e., some might recount only high-level essential plot details, whereas others might recount low-level details instead (or in addition). The second clear pattern present in every individual participant's recall correlation matrix was that, unlike in the episode correlation matrix, there were substantial off-diagonal correlations. Whereas each event in the original episode was (largely) separable from the others (Fig. 2B), in transforming those separable events into memory, participants appeared to be integrating across multiple events, blending elements of previously recalled and not-yet-recalled content into each newly recalled event (Figs. 2E, S4; also see Howard et al., 2012; Manning, 2019; Manning et al., 2011).

The above results demonstrate that topic models capture the dynamic conceptual content of

199 the episode and participants' recalls of the episode. Further, the episode and recalls exhibit event  
200 boundaries that can be identified automatically using HMMs to segment the dynamic content.  
201 Next, we asked whether some correspondence might be made between the specific content of  
202 the events the participants experienced in the episode, and the events they later recalled. We  
203 labeled each recalled event as matching the episode event with the most similar (i.e., most highly  
204 correlated) topic vector (Figs. 2G, S5). This yielded a sequence of "presented" events from the  
205 original episode, and a (potentially differently ordered) sequence of "recalled" events for each  
206 participant. Analogous to classic list-learning studies, we can then examine participants' recall  
207 sequences by asking which events they tended to recall first (probability of first recall; Fig. 3A;  
208 Atkinson and Shiffrin, 1968; Postman and Phillips, 1965; Welch and Burnett, 1924); how participants  
209 most often transitioned between recalls of the events as a function of the temporal distance between  
210 them (lag-conditional response probability; Fig. 3B; Kahana, 1996); and which events they were  
211 likely to remember overall (serial position recall analyses; Fig. 3C; Murdock, 1962). Some of the  
212 patterns we observed appeared to be similar to classic effects from the list-learning literature.  
213 For example, participants had a higher probability of initiating recall with early events (Fig. 3A)  
214 and a higher probability of transitioning to neighboring events with an asymmetric forward bias  
215 (Fig. 3B). However, unlike what is typically observed in list-learning studies, we did not observe  
216 patterns comparable to the primacy or recency serial position effects (Fig. 3C). We hypothesized  
217 that participants might be leveraging meaningful narrative associations and references over long  
218 timescales throughout the episode.

219 Clustering scores are often used by memory researchers to characterize how people organize  
220 their memories of words on a studied list (for review, see Polyn et al., 2009). We defined analogous  
221 measures to characterize how participants organized their memories for episodic events (see  
222 *Methods* for details). Temporal clustering refers to the extent to which participants group their recall  
223 responses according to encoding position. Overall, we found that sequentially viewed episode  
224 events tended to appear nearby in participants' recall event sequences (mean clustering score: 0.767,  
225 SEM: 0.029). Participants with higher temporal clustering scores tended to exhibit better overall  
226 memory for the episode, according to both Chen et al. (2017)'s hand-counted numbers of recalled

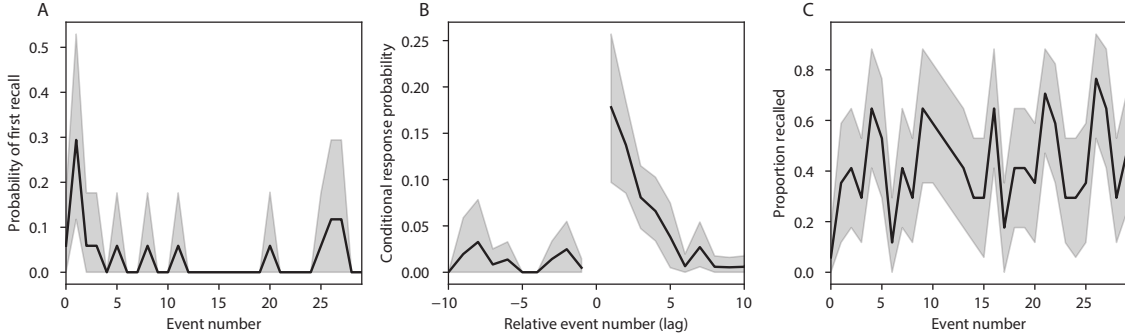


**Figure 3: Naturalistic extensions of classic list-learning memory analyses.** **A.** The probability of first recall as a function of the serial position of the event in the episode. **B.** The probability of recalling each event, conditioned on having most recently recalled the event *lag* events away in the episode. **C.** The proportion of participants who recalled each event, as a function of the serial position of the events in the episode. All panels: error ribbons denote bootstrap-estimated standard error of the mean.

scenes from the episode (Pearson's  $r(15) = 0.62, p = 0.008$ ) and the numbers of episode events that best-matched at least one recalled event (i.e., model-estimated number of recalled events; Pearson's  $r(15) = 0.49, p = 0.0046$ ). Semantic clustering measures the extent to which participants cluster their recall responses according to semantic similarity. We found that participants tended to recall semantically similar episode events together (mean clustering score: 0.787, SEM: 0.018), and that semantic clustering score was also related to both hand-annotated (Pearson's  $r(15) = 0.65, p = 0.004$ ) and model-estimated (Pearson's  $r(15) = 0.61, p = 0.0092$ ) numbers of recalled events.

The above analyses illustrate how our framework for characterizing the dynamic conceptual content of naturalistic episodes enables us to carry out analyses that have traditionally been applied to much simpler list-learning paradigms. However, perhaps the most interesting aspects of memory for naturalistic episodes are those that have no list-learning analogs. The nuances of how one's memory for an event might capture some details, yet distort or neglect others, is central to how we use our memory systems in daily life. Yet when researchers study memory in highly simplified paradigms, those nuances are not typically observable. We next developed two novel continuous metrics, termed precision and distinctiveness, aimed at characterizing distortions in the conceptual content of individual recalled events, and the conceptual overlap between how people described different events.

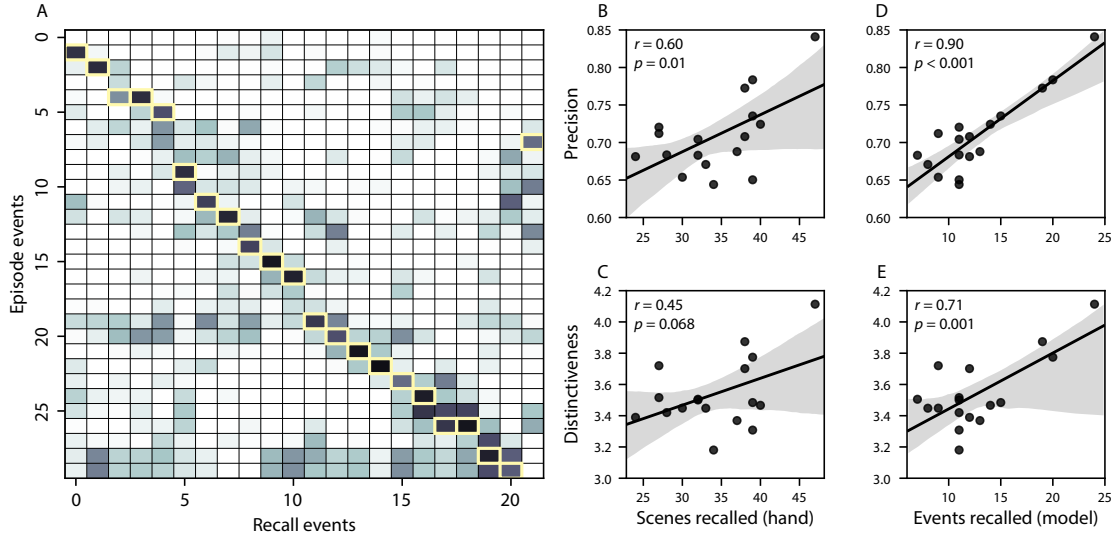


**Figure 4: Novel content-based metrics of naturalistic memory: precision and distinctiveness.** **A.** The episode-recall correlation matrix for a representative participant (P17). The yellow boxes highlight the maximum correlation in each column. The example participant’s overall precision score was computed as the average across correlation values in the yellow boxes. Their distinctiveness score was computed as the average (over recall events) of the z-scored (within column) event precisions. **B.** The (Pearson’s) correlation between precision and hand-counted number of recalled scenes. **C.** The correlation between distinctiveness and hand-counted number of recalled scenes. **D.** The correlation between precision and the number of recalled episode events, as determined by our model. **E.** The correlation between distinctiveness and the number of recalled episode events, as determined by our model.

244     *Precision* is intended to capture the “completeness” of recall, or how fully the presented content  
245     was recapitulated in a participant’s recounting. We define a recall event’s precision as the maximum  
246     correlation between the topic proportions of that recall event and any episode event (Fig. 4). In  
247     other words, given that a recalled event best matches a particular episode event, more precisely  
248     recalled events overlap more strongly with the conceptual content of the original episode event.  
249     When a given event is assigned a blend of several topics, as is often the case (Fig. 2), a high precision  
250     score requires recapitulating the relative topic proportions during recall.

251     *Distinctiveness* is intended to capture the “specificity” of recall. In other words, distinctiveness  
252     quantifies the extent to which a given recalled event reflects the most similar episode event over  
253     and above its reflection of other episode events. Intuitively, distinctiveness is like a normalized  
254     variant of our precision metric. Whereas precision solely measures how much detail about an  
255     episode was captured in someone’s recall, distinctiveness penalizes details that also pertain to  
256     other episode events. We define the distinctiveness of an event’s recall as its precision expressed in  
257     standard deviation units with respect to other episode events. Specifically, for a given recall event,  
258     we compute the correlation between its topic vector and that of each episode event. This yields a  
259     distribution of correlation coefficients (one per episode event). We subtract the mean and divide by  
260     the standard deviation of this distribution to z-score the coefficients. The maximum value in this  
261     distribution (which, by definition, belongs to the episode event that best matches the given recall  
262     event) is that recall event’s distinctiveness score. In this way, recall events that match one episode  
263     event far better than all other episode events will receive a high distinctiveness score. By contrast,  
264     a recall event that matches all episode events roughly equally will receive a comparatively low  
265     distinctiveness score.

266     In addition to examining how precisely and distinctively participants recalled individual events,  
267     one may also use these metrics to summarize each participant’s performance by averaging across  
268     a participant’s event-wise precision or distinctiveness scores. This enables us to quantify how  
269     precisely a participant tended to recall subtle within-event details, as well as how specific (dis-  
270     tinctive) those details were to individual events from the episode. Participants’ average precision  
271     and distinctiveness scores were strongly correlated ( $r(15) = 0.90, p < 10^{-5}$ ). This indicates that

272 participants who tended to precisely recount low-level details of episode events also tended to do  
273 so in an event-specific way (e.g., as opposed to detailing recurring themes that were present in  
274 most or all episode events; this behavior would have resulted in high precision but low distinctiveness). We found that, across participants, higher precision scores were positively correlated with  
275 the numbers of both hand-annotated scenes ( $r(15) = 0.60, p = 0.010$ ) and model-estimated events  
276 ( $r(15) = 0.90, p < 0.001$ ) that participants recalled. Participants' average distinctiveness scores  
277 were also correlated with both the hand-annotated ( $r(15) = 0.45, p = 0.068$ ) and model-estimated  
278 ( $r(15) = 0.71, p = 0.001$ ) numbers of recalled events.

280 Examining individual recalls of the same episode event can provide insights into how the above  
281 precision and distinctiveness scores may be used to characterize similarities and differences in how  
282 different people describe the same shared experience. In Figure 5, we compare recalls for the same  
283 episode event from the participants with the highest (P17) and lowest (P6) precision scores. From  
284 the HMM-identified episode event boundaries, we recovered the set of annotations describing the  
285 content of a single episode event (event 22; Fig. 5C), and divided them into different color-coded  
286 sections for each action or feature described. Next, we used an analogous approach to identify  
287 the set of sentences comprising the corresponding recall event from each of the two example  
288 participants (Fig. 5D). We then colored all words describing actions and features in the transcripts  
289 shown in Panel D according to the color-coded annotations in Panel C. Visual comparison of these  
290 example recalls reveals that the more precise recall captures more of the episode event's content,  
291 and in greater detail.

292 Figure 5 also similarly illustrates the differences between high and low distinctiveness scores.  
293 We extracted the set of sentences comprising the most distinctive recall event (P9) and least distinc-  
294 tive recall event (P6) corresponding to the example episode event shown in Panel C (event 22). We  
295 also extracted the annotations for all episode events whose content these participants' single recall  
296 events described . We assigned each episode event a unique color (Fig. 5E), and colored each recall  
297 sentence (Panel F) according to the episode events they best matched. Visual inspection of Panel F  
298 reveals that the most distinctive recall's content is tightly concentrated around event 22, whereas  
299 the least distinctive recall incorporates content from a much wider range of episode events.

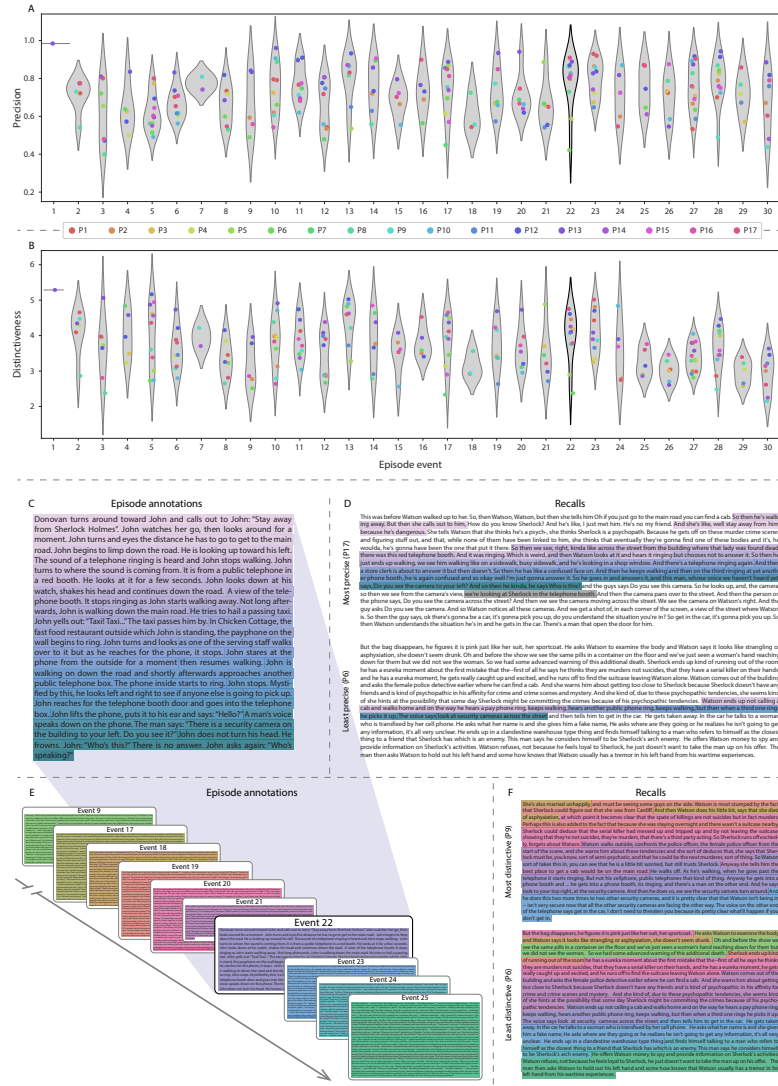


**Figure 5: Precision reflects the completeness of recall, whereas distinctiveness reflects recall specificity.** A. Recall precision by episode event. Grey violin plots display kernel density estimates for the distribution of recall precision scores for a single episode event. Colored dots within each violin plot represent individual participants' recall precision for the given event. Episode events are ordered along the x-axis by the average precision with which they were remembered. B. The set of "Narrative Details" episode annotations (generated by Chen et al., 2017) for scenes comprising an example episode event (22) identified by the HMM. Each action or feature is highlighted in a different color. C. Excerpts from the most precise (P17) and least precise (P6) participants' recalls of episode event 22. Descriptions of specific actions or features reflecting those highlighted in Panel B are highlighted in the corresponding color. The text highlighted in gray denotes a (rare) false recall. The unhighlighted text denotes correctly recalled information about other episode events. D. Recall distinctiveness by episode event. Kernel density estimates for each episode event's distribution of recall distinctiveness scores, analogous to Panel A. E. The sets of "Narrative Details" episode annotations (generated by Chen et al., 2017) for scenes comprising episode events described by the example participants in Panel F. Each event's text is highlighted in a different color. F. The sentences comprising the most distinctive (P9) and least distinctive (P6) participants' recalls of episode event 22. Sections of recall describing each episode event in Panel E are highlighted with the corresponding color.

300      The preceding analyses sought to characterize how participants' recounts of individual  
301    episode events captured the low-level details of each event. Next we sought to characterize how  
302    participants' recounts of the full episode captured its high-level essence— i.e., the shape of the  
303    episode's trajectory through word embedding (topic) space. To visualize the essence of the episode  
304    and each participant's recall trajectory (Heusser et al., 2018b), we projected the topic proportions  
305    matrices for the episode and recalls onto a shared two-dimensional space using Uniform Manifold  
306    Approximation and Projection (UMAP; McInnes et al., 2018). In this lower-dimensional space,  
307    each point represents a single episode or recall event, and the distances between the points reflect  
308    the distances between the events' associated topic vectors (Fig. 6). In other words, events that are  
309    nearer to each other in this space are more semantically similar, and those that are farther apart are  
310    less so.

311      Visual inspection of the episode and recall topic trajectories reveals a striking pattern. First, the  
312    topic trajectory of the episode (which reflects its dynamic content; Fig. 6A) is captured nearly per-  
313    fectly by the averaged topic trajectories of participants' recalls (Fig. 6B). To assess the consistency  
314    of these recall trajectories across participants, we asked: given that a participant's recall trajectory  
315    had entered a particular location in the reduced topic space, could the position of their *next* recalled  
316    event be predicted reliably? For each location in the reduced topic space, we computed the set of  
317    line segments connecting successively recalled events (across all participants) that intersected that  
318    location (see *Methods* for additional details). We then computed (for each location) the distribu-  
319    tion of angles formed by the lines defined by those line segments and a fixed reference line (the  
320    *x*-axis). Rayleigh tests revealed the set of locations in topic space at which these across-participant  
321    distributions exhibited reliable peaks (blue arrows in Fig. 6B reflect significant peaks at  $p < 0.05$ ,  
322    corrected). We observed that the locations traversed by nearly the entire episode trajectory exhib-  
323    ited such peaks. In other words, participants' recalls exhibited similar trajectories to each other  
324    that also matched the trajectory of the original episode (Fig. 6C). This is especially notable when  
325    considering the fact that the numbers of events participants recalled (dots in Fig. 6C) varied con-  
326    siderably across people, and that every participant used different words to describe what they had  
327    remembered happening in the episode. Differences in the numbers of remembered events appear

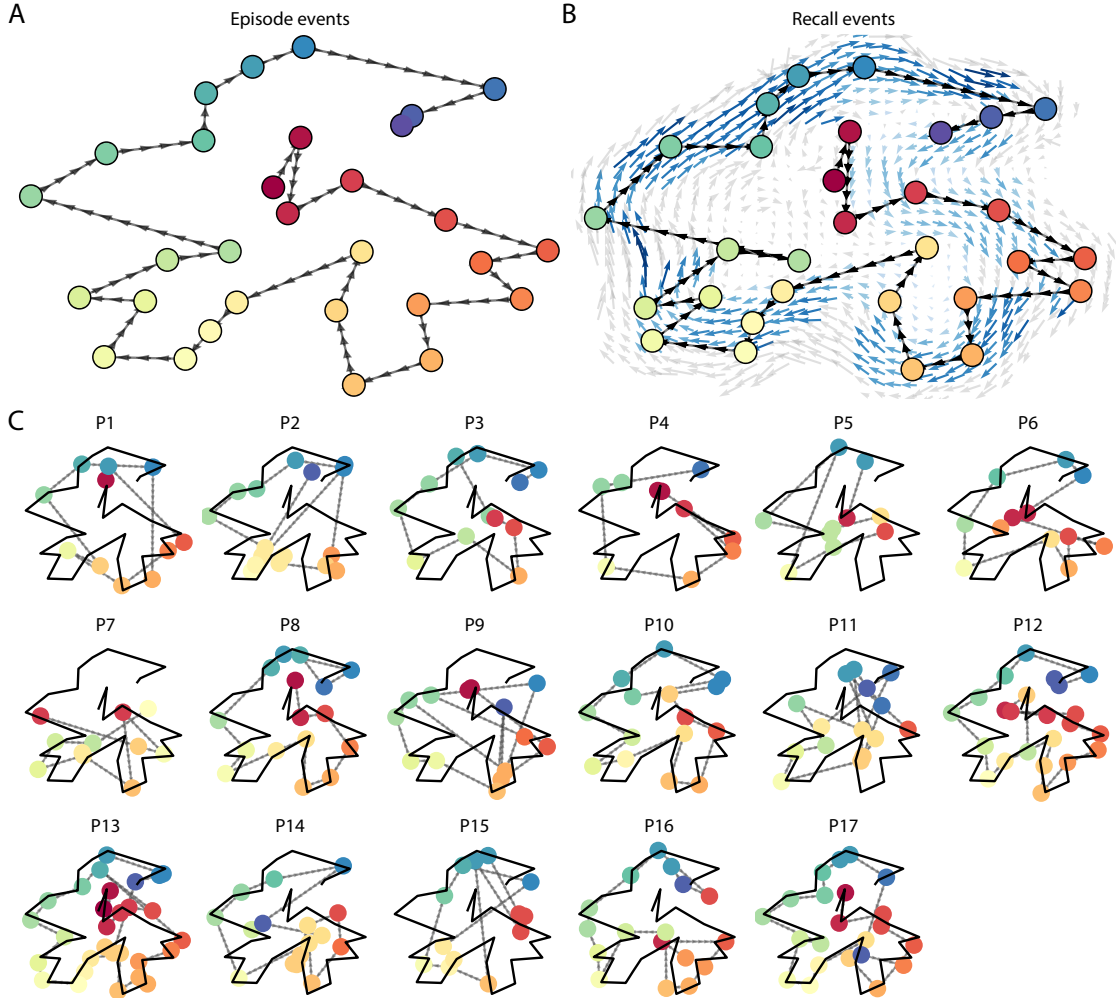


**Figure 6: Trajectories through topic space capture the dynamic content of the episode and recalls.** All panels: the topic proportion matrices have been projected onto a shared two-dimensional space using UMAP. **A.** The two-dimensional topic trajectory taken by the episode of *Sherlock*. Each dot indicates an event identified using the HMM (see *Methods*); the dot colors denote the order of the events (early events are in red; later events are in blue), and the connecting lines indicate the transitions between successive events. **B.** The average two-dimensional trajectory captured by participants' recall sequences, with the same format and coloring as the trajectory in Panel A. To compute the event positions, we matched each recalled event with an event from the original episode (see *Results*), and then we averaged the positions of all events with the same label. The arrows reflect the average transition direction through topic space taken by any participants whose trajectories crossed that part of topic space; blue denotes reliable agreement across participants via a Rayleigh test ( $p < 0.05$ , corrected). **C.** The recall topic trajectories (gray) taken by each individual participant (P1–P17). The episode's trajectory is shown in black for reference. Here, events (dots) are colored by their matched episode event (Panel A).

328 in participants' trajectories as differences in the sampling resolution along the trajectory. We note  
329 that this framework also provides a means of disentangling classic "proportion recalled" measures  
330 (i.e., the proportion of episode events described in participants' recalls) from participants' abilities  
331 to recapitulate the episode's essence (i.e., the similarity between the shapes of the original episode  
332 trajectory and that defined by each participant's recounting of the episode).

333 In addition to enabling us to visualize the episode's high-level essence, describing the episode  
334 as a geometric trajectory also enables us to drill down to individual words and quantify how each  
335 word relates to the memorability of each event. This provides another approach to examining  
336 participants' recall for low-level details beyond the precision and distinctiveness measures we  
337 defined above. The results displayed in Figures 3C and 5A suggest that certain events were  
338 remembered better than others. Given this, we next asked whether the events were generally  
339 remembered precisely or imprecisely tended to reflect particular content. Because our analysis  
340 framework projects the dynamic episode content and participants' recalls into a shared space, and  
341 because the dimensions of that space represent topics (which are, in turn, sets of weights over  
342 known words in the vocabulary), we are able to recover the weighted combination of words that  
343 make up any point (i.e., topic vector) in this space. We first computed the average precision with  
344 which participants recalled each of the 30 episode events (Fig. 7A; note that this result is analogous  
345 to a serial position curve created from our precision metric). We then computed a weighted average  
346 of the topic vectors for each episode event, where the weights reflected how precisely each event  
347 was recalled. To visualize the result, we created a "wordle" image (Mueller et al., 2018) where  
348 words weighted more heavily by more precisely-remembered topics appear in a larger font (Fig. 7B,  
349 green box). Across the full episode, content that weighted heavily on topics and words central to  
350 the major foci of the episode (e.g., the names of the two main characters, "Sherlock" and "John,"  
351 and the address of a major recurring location, "221B Baker Street") were best remembered. An  
352 analogous analysis revealed which themes were less-precisely remembered. Here in computing  
353 the weighted average over events' topic vectors, we weighted each event in *inverse* proportion to  
354 its average precision (Fig. 7B, red box). The least precisely remembered episode content reflected  
355 information that was extraneous to the episode's essence, such as the proper names of relatively

356 minor characters (e.g., "Mike," "Molly," and "Lestrade") and locations (e.g., "St. Bartholomew's  
357 Hospital").

358 A similar result emerged from assessing the topic vectors for individual episode and recall  
359 events (Fig. 7C). Here, for each of the three most and least precisely remembered episode events, we  
360 have constructed two wordles: one from the original episode event's topic vector (left) and a second  
361 from the average recall topic vector for that event (right). The three most precisely remembered  
362 events (circled in green) correspond to scenes integral to the central plot-line: a mysterious figure  
363 spying on John in a phone booth; John meeting Sherlock at Baker St. to discuss the murders; and  
364 Sherlock laying a trap to catch the killer. Meanwhile, the least precisely remembered events (circled  
365 in red) reflect scenes that comprise minor plot points: a video of singing cartoon characters that  
366 participants viewed in an introductory clip prior to the main episode; John asking Molly about  
367 Sherlock's habit of over-analyzing people; and Sherlock noticing evidence of Anderson's and  
368 Donovan's affair.

369 The results thus far inform us about which aspects of the dynamic content in the episode partic-  
370 ipants watched were preserved or altered in participants' memories. We next carried out a series of  
371 analyses aimed at understanding which brain structures might facilitate these preservations and  
372 transformations between the participants' shared experience of watching the episode and their  
373 subsequent memories of the episode. In the first analysis, we sought to identify brain structures  
374 that were sensitive to the dynamic unfolding of the episode's content, as characterized by its topic  
375 trajectory. We used a searchlight procedure to identify clusters of voxels whose activity patterns  
376 displayed a proximal temporal correlation structure (as participants watched the episode) match-  
377 ing that of the original episode's topic proportions (Fig. 8A; see *Methods* for additional details). In a  
378 second analysis, we sought to identify brain structures whose responses (during episode viewing)  
379 reflected how each participant would later structure their *recounting* of the episode. We used a  
380 searchlight procedure to identify clusters of voxels whose proximal temporal correlation matrices  
381 matched that of the topic proportions matrix for each participant's recall transcript (Figs. 8B; see  
382 *Methods* for additional details). To ensure our searchlight procedure identified regions *specifically*  
383 sensitive to the temporal structure of the episode or recalls (i.e., rather than those with a tem-

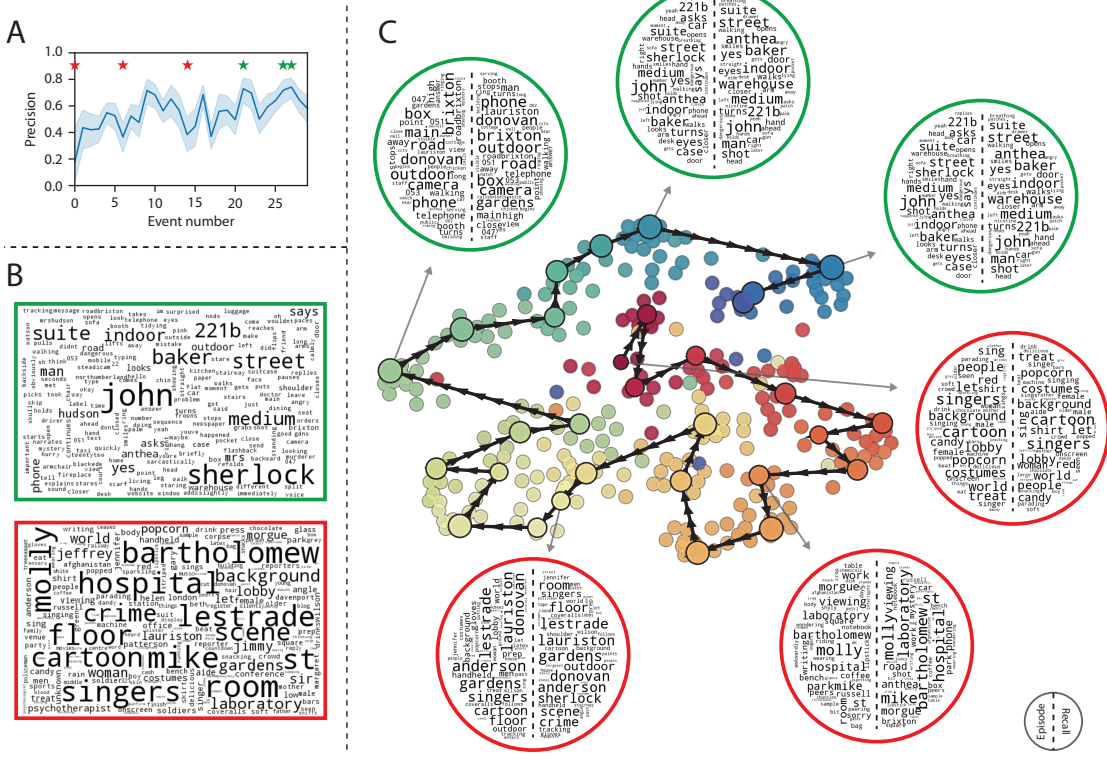


**Figure 7: Language used in the most and least precisely remembered events.** **A.** Average precision (episode event-recall event topic vector correlation) across participants for each episode event. Here we defined each episode event's precision for each participant as the correlation between its topic vector and the most-correlated recall event's topic vector from that participant. Error bars denote bootstrap-derived across-participant 95% confidence intervals. The stars denote the three most precisely remembered events (green) and least precisely remembered events (red). **B.** Wordles comprising the top 200 highest-weighted words reflected in the weighted-average topic vector across episode events. Green: episode events were weighted by their precision (Panel A). Red: episode events were weighted by the inverse of their precision. **C.** The set of all episode and recall events is projected onto the two-dimensional space derived in Figure 6. The dots outlined in black denote episode events (dot size is proportional to each event's average precision). The dots without black outlines denote individual recall events from each participant. All dots are colored using the same scheme as Figure 6A. Wordles for several example events are displayed (green: three most precisely remembered events; red: three least precisely remembered events). Within each circular wordle, the left side displays words associated with the topic vector for the episode event, and the right side displays words associated with the (average) recall event topic vector, across all recall events matched to the given episode event.

384 poral autocorrelation length similar to that of the episode and recalls), we performed a phase  
385 shift-based permutation correction (see *Methods* for additional details). As shown in Figure 8C,  
386 the episode-driven searchlight analysis revealed a distributed network of regions that may play  
387 a role in processing information relevant to the narrative structure of the episode. Similarly, the  
388 recall-driven searchlight analysis revealed a second network of regions (Fig. 8D) that may facil-  
389 itate a person-specific transformation of one's experience into memory. The top ten Neurosynth  
390 terms (Yarkoni et al., 2011) associated with each (unthresholded) map are displayed in each panel.  
391 In identifying regions whose responses to ongoing experiences reflect how those experiences will  
392 be remembered later, this latter analysis extends classic *subsequent memory effect analyses* (e.g., Paller  
393 and Wagner, 2002) to the domain of naturalistic experiences.

394 The searchlight analyses described above yielded two distributed networks of brain regions,  
395 whose activity timecourses tracked with the temporal structure of the episode (Fig. 8C) or par-  
396 ticipants' subsequent recalls (Fig. 8D). We next sought to gain greater insight into the structures  
397 and functional networks our results reflected. To accomplish this, we performed an additional,  
398 exploratory analysis using **Neurosynth** (Yarkoni et al., 2011). Given an arbitrary statistical map as  
399 input, **Neurosynth** performs a massive automated meta-analysis, returning a ranked list of terms  
400 reported in papers with similar significance maps. We ran **Neurosynth** on the significance maps  
401 for the episode- and recall-driven searchlight analyses. These maps, along with the 10 terms with  
402 maximally similar meta-analysis images identified by **Neurosynth** are shown in Figure 8.

## 403 Discussion

404 Explicitly modeling the dynamic content of a naturalistic stimulus and participants' memories  
405 enabled us to connect the present study of naturalistic recall with an extensive prior literature that  
406 has used list-learning paradigms to study memory (for review see Kahana, 2012), as in Figure 3.  
407 We found some similarities between how participants in the present study recounted a television  
408 episode and how participants typically recall memorized random word lists. However, our broader  
409 claim is that word lists miss out on fundamental aspects of naturalistic memory more like the sort

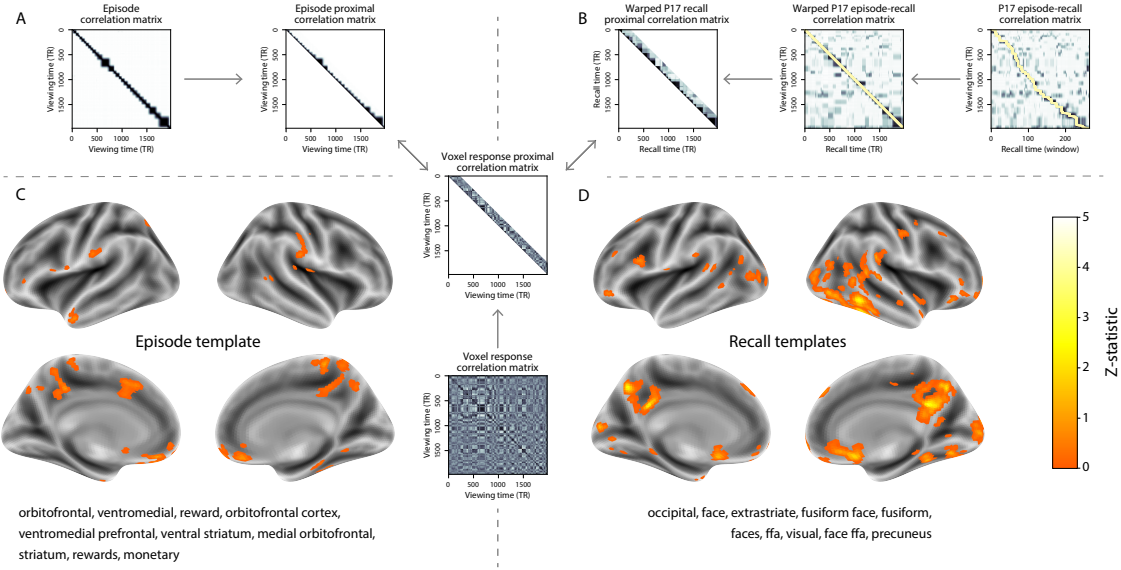


**Figure 8: Brain structures that underlie the transformation of experience into memory.** **A.** We isolated the proximal diagonals from the upper triangle of the episode correlation matrix, and applied this same diagonal mask to the voxel response correlation matrix for each cube of voxels in the brain. We then searched for brain regions whose activation timeseries consistently exhibited a similar proximal correlational structure to the episode model, across participants. **B.** We used dynamic time warping (Berndt and Clifford, 1994) to align each participant's recall timeseries to the TR timeseries of the episode. We then applied the same diagonal mask used in Panel A to isolate the proximal temporal correlations and searched for brain regions whose activation timeseries for an individual consistently exhibited a similar proximal correlational structure to each individual's recall. **C.** We identified a network of regions sensitive to the narrative structure of participants' ongoing experience. The map shown is thresholded at  $p < 0.05$ , corrected. The top ten Neurosynth terms displayed in the panel were computed using the unthresholded map. **D.** We also identified a network of regions sensitive to how individuals would later structure the episode's content in their recalls. The map shown is thresholded at  $p < 0.05$ , corrected. The top ten Neurosynth terms displayed in the panel were computed using the unthresholded map.

410 of memory we rely on in everyday life. For example, there are no random word list analogs of  
411 character interactions, conceptual dependencies between temporally distant episode events, the  
412 sense of solving a mystery that pervades the *Sherlock* episode, or the myriad other features of the  
413 episode that convey deep meaning and capture interest. Nevertheless, each of these properties  
414 affects how people process and engage with the episode as they are watching it, and how they  
415 remember it later. The overarching goal of the present study is to characterize how the rich  
416 dynamics of the episode affect the rich behavioral and neural dynamics of how people remember  
417 it.

418 Our work casts remembering as reproducing (behaviorally and neurally) the topic trajectory,  
419 or “shape,” of an experience. When we characterized memory for a television episode using this  
420 framework, we found that every participant’s recounting of the episode recapitulated the low  
421 spatial frequency details of the shape of its trajectory through topic space (Fig. 6). We termed  
422 this narrative scaffolding the episode’s *essence*. Where participants’ behaviors varied most was  
423 in their tendencies to recount specific low-level details from each episode event. Geometrically,  
424 this appears as high spatial frequency distortions in participants’ recall trajectories relative to the  
425 trajectory of the original episode (Fig. 7). We developed metrics to characterize the precision  
426 (recovery of any and all event-level information) and distinctiveness (recovery of event-specific  
427 information). We also used word cloud visualizations to interpret the details of these event-level  
428 distortions.

429 The neural analyses we carried out (Fig. 8) also leveraged our geometric framework for char-  
430 acterizing the shapes of the episode and participants’ recounts. We identified one network  
431 of regions whose responses tracked with temporal correlations in the conceptual content of the  
432 episode (as quantified by topic models applied to a set of annotations about the episode). This  
433 network included orbitofrontal cortex, ventromedial prefrontal cortex, striatum, among others. As  
434 reviewed by Ranganath and Ritchey (2012), several of these regions are members of the *anterior*  
435 *temporal system*, which has been implicated in assessing and processing the familiarity of ongoing  
436 experiences, emotions, social cognition, and reward. A second network we identified tracked with  
437 temporal correlations in the idiosyncratic conceptual content of participants’ subsequent recount-

438 ings of the episode. This network included occipital cortex, extrastriate cortex, fusiform gyrus, and  
439 the precuneus. Several of these regions are members of the *posterior medial system* (Ranganath and  
440 Ritchey, 2012), which has been implicated in matching incoming cues about the current situation  
441 to internally maintained *situation models* that specify the parameters and expectations inherent to  
442 the current situation (also see Zacks et al., 2007; Zwaan and Radvansky, 1998). Taken together, our  
443 results support the notion that these two (partially overlapping) networks work in coordination  
444 to make sense of our ongoing experiences, distort them in a way that links them with our prior  
445 knowledge and experiences, and encodes those distorted representations into memory for our later  
446 use.

447 Our general approach draws inspiration from prior work aimed at elucidating the neural and  
448 behavioral underpinnings of how we process dynamic naturalistic experiences and remember them  
449 later. Our approach to identifying neural responses to naturalistic stimuli (including experiences)  
450 entails building an explicit model of the stimulus dynamics and searching for brain regions whose  
451 responses are consistent with the model (also see Huth et al., 2016, 2012). In prior work, a  
452 series of studies from Uri Hasson’s group (Baldassano et al., 2017; Chen et al., 2017; Lerner et al.,  
453 2011; Simony et al., 2016; Zadbood et al., 2017) have developed a clever alternative approach:  
454 rather than building an explicit stimulus model, these studies instead search for brain responses  
455 (while experiencing the stimulus) that are reliably similar across individuals. So called *inter-*  
456 *subject correlation* (ISC) and *inter-subject functional connectivity* (ISFC) analyses effectively treat other  
457 people’s brain responses to the stimulus as a “model” of how its features change over time (also  
458 see Simony and Chang, 2020). These purely brain-driven approaches are well-suited to identifying  
459 which brain structures exhibit similar stimulus-driven responses across individuals. Further,  
460 because neural response dynamics are observed data (rather than model approximations), such  
461 approaches do not require a detailed understanding of which stimulus properties or features might  
462 be driving the observed responses. However, this also means that the specific stimulus features  
463 driving those responses are typically opaque to the researcher. Our approach is complementary.  
464 By explicitly modeling the stimulus dynamics, we are able to relate specific stimulus features to  
465 behavioral and neural dynamics. However, when our model fails to accurately capture the stimulus

466 dynamics that are truly driving behavioral and neural responses, our approach necessarily yields  
467 an incomplete characterization of the neural basis of the processes we are studying.

468 Other recent work has used HMMs to discover latent event structure in neural responses  
469 to naturalistic stimuli (Baldassano et al., 2017). By applying HMMs to our explicit models of  
470 stimulus and memory dynamics, we gain a more direct understanding of those state dynamics.  
471 For example, we found that although the events comprising each participant’s recalls recapitulated  
472 the episode’s essence, participants differed in the *resolution* of their recounting of low-level details.  
473 In turn, these individual behavioral differences were reflected in differences in neural activity  
474 dynamics as participants watched the television episode.

475 Our approach also draws inspiration from the growing field of word embedding models. The  
476 topic models (Blei et al., 2003) we used to embed text from the episode annotations and participants’  
477 recall transcripts are just one of many models that have been studied in an extensive literature.  
478 The earliest approaches to word embedding, including latent semantic analysis (Landauer and  
479 Dumais, 1997), used word co-occurrence statistics (i.e., how often pairs of words occur in the  
480 same documents contained in the corpus) to derive a unique feature vector for each word. The  
481 feature vectors are constructed so that words that co-occur more frequently have feature vectors  
482 that are closer (in Euclidean distance). Topic models are essentially an extension of those early  
483 models, in that they attempt to explicitly model the underlying causes of word co-occurrences by  
484 automatically identifying the set of themes or topics reflected across the documents in the corpus.  
485 More recent work on these types of semantic models, including word2vec (Mikolov et al., 2013),  
486 the Universal Sentence Encoder (Cer et al., 2018), GPT-2 (Radford et al., 2019), and GTP-3 (Brown  
487 et al., 2020) use deep neural networks to attempt to identify the deeper conceptual representations  
488 underlying each word. Despite the growing popularity of these sophisticated deep learning-based  
489 embedding models, we chose to prioritize interpretability of the embedding dimensions (e.g.,  
490 Fig. 7) over raw performance (e.g., with respect to some predefined benchmark). Nevertheless, we  
491 note that our general framework is, in principle, robust to the specific choice of language model  
492 as well as other aspects of our computational pipeline. For example, the word embedding model,  
493 timeseries segmentation model, and the episode-recall matching function could each be customized

494 to suit a particular question space or application. Indeed, for some questions, interpretability of  
495 the embeddings may not be a priority, and thus other text embedding approaches (including the  
496 deep learning-based models described above) may be preferable. Further work will be needed to  
497 explore the influence of particular models on our framework’s predictions and performance.

498 Our work has broad implications for how we characterize and assess memory in real-world  
499 settings, such as the classroom or physician’s office. For example, the most commonly used  
500 classroom evaluation tools involve simply computing the proportion of correctly answered exam  
501 questions. Our work indicates that this approach is only loosely related to what educators might  
502 really want to measure: how well did the students understand the key ideas presented in the  
503 course? Under this typical framework of assessment, the same exam score of 50% could be ascribed  
504 to two very different students: one who attended to the full course but struggled to learn more than  
505 a broad overview of the material, and one who attended to only half of the course but understood  
506 the attended material perfectly. Instead, one could apply our computational framework to build  
507 explicit dynamic content models of the course material and exam questions. This approach would  
508 provide a more nuanced and specific view into which aspects of the material students had learned  
509 well (or poorly). In clinical settings, memory measures that incorporate such explicit content  
510 models might also provide more direct evaluations of patients’ memories, and of doctor-patient  
511 interactions.

## 512 Methods

### 513 Paradigm and data collection

514 Data were collected by Chen et al. (2017). In brief, participants ( $n = 22$ ) viewed the first 48 minutes  
515 of “A Study in Pink,” the first episode of the BBC television show *Sherlock*, while fMRI volumes  
516 were collected (TR = 1500 ms). Participants were pre-screened to ensure they had never seen any  
517 episode of the show before. The stimulus was divided into a 23 min (946 TR) and a 25 min (1030 TR)  
518 segment to mitigate technical issues related to the scanner. After finishing the clip, participants

519 were instructed to (quoting from Chen et al., 2017) “describe what they recalled of the [episode]  
520 in as much detail as they could, to try to recount events in the original order they were viewed  
521 in, and to speak for at least 10 minutes if possible but that longer was better. They were told that  
522 completeness and detail were more important than temporal order, and that if at any point they  
523 realized they had missed something, to return to it. Participants were then allowed to speak for  
524 as long as they wished, and verbally indicated when they were finished (e.g., ‘I’m done’).” Five  
525 participants were dropped from the original dataset due to excessive head motion (2 participants),  
526 insufficient recall length (2 participants), or falling asleep during stimulus viewing (1 participant),  
527 resulting in a final sample size of  $n = 17$ . For additional details about the testing procedures  
528 and scanning parameters, see Chen et al. (2017). The testing protocol was approved by Princeton  
529 University’s Institutional Review Board.

530 After preprocessing the fMRI data and warping the images into a standard ( $3 \text{ mm}^3$  MNI) space,  
531 the voxel activations were z-scored (within voxel) and spatially smoothed using a 6 mm (full width  
532 at half maximum) Gaussian kernel. The fMRI data were also cropped so that all episode-viewing  
533 data were aligned across participants. This included a constant 3 TR (4.5 s) shift to account for the  
534 lag in the hemodynamic response. (All of these preprocessing steps followed Chen et al., 2017,  
535 where additional details may be found.)

536 The video stimulus was divided into 1,000 fine-grained “scenes” and annotated by an inde-  
537 pendent coder. For each of these 1,000 scenes, the following information was recorded: a brief  
538 narrative description of what was happening, the location where the scene took place, whether  
539 that location was indoors or outdoors, the names of all characters on-screen, the name(s) of the  
540 character(s) in focus in the shot, the name(s) of the character(s) currently speaking, the camera  
541 angle of the shot, a transcription of any text appearing on-screen, and whether or not there was  
542 music present in the background. Each scene was also tagged with its onset and offset time, in  
543 both seconds and TRs.

544 **Data and code availability**

545 The fMRI data we analyzed are available online [here](#). The behavioral data and all of our analysis  
546 code may be downloaded [here](#).

547 **Statistics**

548 All statistical tests performed in the behavioral analyses were two-sided. All statistical tests per-  
549 formed in the neural data analyses were two-sided, except for the permutation-based thresholding,  
550 which was one-sided. In this case, we were specifically interested in identifying voxels whose acti-  
551 vation time series reflected the temporal structure of the episode and recall trajectories to a *greater*  
552 extent than that of the phase-shifted trajectories.

553 **Modeling the dynamic content of the episode and recall transcripts**

554 **Topic modeling**

555 The input to the topic model we trained to characterize the dynamic content of the episode  
556 comprised 998 hand-generated annotations of short (mean: 2.96s) scenes spanning the video  
557 clip (Chen et al., 2017 generated 1000 annotations total; we removed two annotations referring to  
558 a break between the first and second scan sessions, during which no fMRI data were collected).  
559 We concatenated the text for all of the annotated features within each segment, creating a “bag of  
560 words” describing each scene and performed some minor preprocessing (e.g., stemming possessive  
561 nouns and removing punctuation). We then re-organized the text descriptions into overlapping  
562 sliding windows spanning (up to) 50 scenes each. In other words, we estimated the “context”  
563 for each scene using the text descriptions of the preceding 25 scenes, the present scene, and the  
564 following 24 scenes. To model the context for scenes near the beginning of the episode (i.e., within  
565 25 scenes of the beginning or end), we created overlapping sliding windows that grew in size  
566 from one scene to the full length. We also tapered the sliding window lengths at the end of the  
567 episode, whereby scenes within fewer than 24 scenes of the end of the episode were assigned

568 sliding windows that extended to the end of the episode. This procedure ensured that each scene's  
569 content was represented in the text corpus an equal number of times.

570 We trained our model using these overlapping text samples with `scikit-learn` (version 0.19.1;  
571 Pedregosa et al., 2011), called from our high-dimensional visualization and text analysis software,  
572 `HyperTools` (Heusser et al., 2018b). Specifically, we used the `CountVectorizer` class to transform  
573 the text from each window into a vector of word counts (using the union of all words across all  
574 scenes as the "vocabulary," excluding English stop words); this yielded a number-of-windows  
575 by number-of-words *word count* matrix. We then used the `LatentDirichletAllocation` class  
576 (`topics=100, method='batch'`) to fit a topic model (Blei et al., 2003) to the word count matrix,  
577 yielding a number-of-windows (1047) by number-of-topics (100) *topic proportions* matrix. The  
578 topic proportions matrix describes the gradually evolving mix of topics (latent themes) present in  
579 each scene. Next, we transformed the topic proportions matrix to match the 1976 fMRI volume  
580 acquisition times. We assigned each topic vector to the timepoint (in seconds) midway between the  
581 beginning of the first scene and the end of the last scene in its corresponding sliding text window.  
582 By doing so, we warped the linear temporal distance between consecutive topic vectors to align  
583 with the inconsistent temporal distance between consecutive annotations (whose durations varied  
584 greatly). We then rescaled these timepoints to 1.5s TR units, and used linear interpolation to  
585 estimate a topic vector for each TR. This resulted in a number-of-TRs (1976) by number-of-topics  
586 (100) matrix.

587 We created similar topic proportions matrices using hand-annotated transcripts of each partic-  
588 ipant's verbal recall of the episode (annotated by Chen et al., 2017). We tokenized the transcript  
589 into a list of sentences, and then re-organized the list into overlapping sliding windows spanning  
590 (up to) 10 sentences each, analogously to how we parsed the episode annotations. In turn, we  
591 transformed each window's sentences into a word count vector (using the same vocabulary as for  
592 the episode model), and then we used the topic model already trained on the episode scenes to  
593 compute the most probable topic proportions for each sliding window. This yielded a number-of-  
594 windows (range: 83–312) by number-of-topics (100) topic proportions matrix for each participant.  
595 These reflected the dynamic content of each participant's recalls. Note: for details on how we

596 selected the episode and recall window lengths and number of topics, see *Supporting Information*  
597 and Figure S1.

598 **Segmenting topic proportions matrices into discrete events using hidden Markov Models**

599 We parsed the topic proportions matrices of the episode and participants' recalls into discrete  
600 events using hidden Markov Models (HMMs; Rabiner, 1989). Given the topic proportions matrix  
601 (describing the mix of topics at each timepoint) and a number of states,  $K$ , an HMM recovers the  
602 set of state transitions that segments the timeseries into  $K$  discrete states. Following Baldassano  
603 et al. (2017), we imposed an additional set of constraints on the discovered state transitions that  
604 ensured that each state was encountered exactly once (i.e., never repeated). We used the BrainIAK  
605 toolbox (Capota et al., 2017) to implement this segmentation.

606 We used an optimization procedure to select the appropriate  $K$  for each topic proportions  
607 matrix. Prior studies on narrative structure and processing have shown that we both perceive  
608 and internally represent the world around us at multiple, hierarchical timescales (e.g., Baldassano  
609 et al., 2017, 2018; Chen et al., 2017; Hasson et al., 2015, 2008; Lerner et al., 2011). However, for the  
610 purposes of our framework, we sought to identify the single timeseries of event-representations  
611 that is emphasized *most heavily* in the temporal structure of the episode and of each participant's  
612 recall. We quantified this as the set of  $K$  states that maximized the similarity between topic vectors  
613 for timepoints comprising each state, while minimizing the similarity between topic vectors for  
614 timepoints across different states. Specifically, we computed (for each matrix)

$$\operatorname{argmax}_K [W_1(a, b)],$$

615 where  $a$  was the distribution of within-state topic vector correlations, and  $b$  was the distribution of  
616 across-state topic vector correlations . We computed the first Wasserstein distance ( $W_1$ ; also known  
617 as *Earth mover's distance*; Dobrushin, 1970; Ramdas et al., 2017) between these distributions for a  
618 large range of possible  $K$ -values (range [2, 50]), and selected the  $K$  that yielded the maximum value.  
619 Figure 2B displays the event boundaries returned for the episode, and Figure S4 displays the event

620 boundaries returned for each participant’s recalls. See Figure S6 for the optimization functions  
621 for the episode and recalls. After obtaining these event boundaries, we created stable estimates  
622 of the content represented in each event by averaging the topic vectors across timepoints between  
623 each pair of event boundaries. This yielded a number-of-events by number-of-topics matrix for  
624 the episode and recalls from each participant.

625 **Naturalistic extensions of classic list-learning analyses**

626 In traditional list-learning experiments, participants view a list of items (e.g., words) and then  
627 recall the items later. Our episode-recall event matching approach affords us the ability to analyze  
628 memory in a similar way. The episode and recall events can be treated analogously to studied and  
629 recalled “items” in a list-learning study. We can then extend classic analyses of memory perfor-  
630 mance and dynamics (originally designed for list-learning experiments) to the more naturalistic  
631 episode recall task used in this study.

632 Perhaps the simplest and most widely used measure of memory performance is *accuracy*—i.e.,  
633 the proportion of studied (experienced) items (in this case, episode events) that the participant later  
634 remembered. Chen et al. (2017) used this method to rate each participant’s memory quality by  
635 computing the proportion of (50, manually identified) scenes mentioned in their recall. We found a  
636 strong across-participants correlation between these independent ratings and the proportion of 30  
637 HMM-identified episode events matched to participants’ recalls (Pearson’s  $r(15) = 0.71, p = 0.002$ ).  
638 We further considered a number of more nuanced memory performance measures that are typically  
639 associated with list-learning studies. We also provide a software package, Quail, for carrying out  
640 these analyses (Heusser et al., 2017).

641 **Probability of first recall (PFR).** PFR curves (Atkinson and Shiffrin, 1968; Postman and Phillips,  
642 1965; Welch and Burnett, 1924) reflect the probability that an item will be recalled first as a function  
643 of its serial position during encoding. To carry out this analysis, we initialized a number-of-  
644 participants (17) by number-of-episode-events (30) matrix of zeros. Then for each participant, we  
645 found the index of the episode event that was recalled first (i.e., the episode event whose topic

646 vector was most strongly correlated with that of the first recall event) and filled in that index in  
647 the matrix with a 1. Finally, we averaged over the rows of the matrix, resulting in a 1 by 30 array  
648 representing the proportion of participants that recalled an event first, as a function of the order of  
649 the event's appearance in the episode (Fig. 3A).

650 **Lag conditional probability curve (lag-CRP).** The lag-CRP curve (Kahana, 1996) reflects the  
651 probability of recalling a given item after the just-recalled item, as a function of their relative  
652 encoding positions (or *lag*). In other words, a lag of 1 indicates that a recalled item was presented  
653 immediately after the previously recalled item, and a lag of -3 indicates that a recalled item came 3  
654 items before the previously recalled item. For each recall transition (following the first recall), we  
655 computed the lag between the current recall event and the next recall event, normalizing by the  
656 total number of possible transitions. This yielded a number-of-participants (17) by number-of-lags  
657 (-29 to +29; 58 lags total excluding lags of 0) matrix. We averaged over the rows of this matrix to  
658 obtain a group-averaged lag-CRP curve (Fig. 3B).

659 **Serial position curve (SPC).** SPCs (Murdock, 1962) reflect the proportion of participants that  
660 remember each item as a function of the items' serial positions during encoding. We initialized  
661 a number-of-participants (17) by number-of-episode-events (30) matrix of zeros. Then, for each  
662 recalled event, for each participant, we found the index of the episode event that the recalled  
663 event most closely matched (via the correlation between the events' topic vectors) and entered a  
664 1 into that position in the matrix. This resulted in a matrix whose entries indicated whether or  
665 not each event was recalled by each participant (depending on whether the corresponding entires  
666 were set to one or zero). Finally, we averaged over the rows of the matrix to yield a 1 by 30 array  
667 representing the proportion of participants that recalled each event as a function of the events'  
668 order appearance in the episode (Fig. 3C).

669 **Temporal clustering scores.** Temporal clustering describes a participant's tendency to organize  
670 their recall sequences by the learned items' encoding positions. For instance, if a participant  
671 recalled the episode events in the exact order they occurred (or in exact reverse order), this would

yield a score of 1. If a participant recalled the events in random order, this would yield an expected score of 0.5. For each recall event transition (and separately for each participant), we sorted all not-yet-recalled events according to their absolute lag (i.e., distance away in the episode). We then computed the percentile rank of the next event the participant recalled. We averaged these percentile ranks across all of the participant’s recalls to obtain a single temporal clustering score for the participant.

**Semantic clustering scores.** Semantic clustering describes a participant’s tendency to recall semantically similar presented items together in their recall sequences. Here, we used the topic vectors for each event as a proxy for its semantic content. Thus, the similarity between the semantic content for two events can be computed by correlating their respective topic vectors. For each recall event transition, we sorted all not-yet-recalled events according to how correlated the topic vector of *the closest-matching episode event* was to the topic vector of the closest-matching episode event to the just-recalled event. We then computed the percentile rank of the observed next recall. We averaged these percentile ranks across all of the participant’s recalls to obtain a single semantic clustering score for the participant.

### Averaging correlations

In all instances where we performed statistical tests involving precision or distinctiveness scores (Fig. 5, we used the Fisher  $z$ -transformation (Fisher, 1925) to stabilize the variance across the distribution of correlation values prior to performing the test. Similarly, when averaging precision or distinctiveness scores, we  $z$ -transformed the scores prior to computing the mean, and inverse  $z$ -transformed the result.

### Visualizing the episode and recall topic trajectories

We used the UMAP algorithm (McInnes et al., 2018) to project the 100-dimensional topic space onto a two-dimensional space for visualization (Figs. 6, 7). To ensure that all of the trajectories were projected onto the *same* lower dimensional space, we computed the low-dimensional embedding

697 on a “stacked” matrix created by vertically concatenating the events-by-topics topic proportions  
698 matrices for the episode, across-participants average recall and all 17 individual participants’ re-  
699 calls. We then separated the rows of the result (a total-number-of-events by two matrix) back into  
700 individual matrices for the episode topic trajectory, across-participant average recall trajectory and  
701 the trajectories for each individual participant’s recalls (Fig. 6). This general approach for dis-  
702 covering a shared low-dimensional embedding for a collections of high-dimensional observations  
703 follows Heusser et al. (2018b).

704 We optimized the manifold space for visualization based on two criteria: First, that the 2D em-  
705 bedding of the episode trajectory should reflect its original 100-dimensional structure as faithfully  
706 as possible. Second, that the path traversed by the embedded episode trajectory should intersect  
707 itself a minimal number of times. The first criteria helps bolster the validity of visual intuitions  
708 about relationships between sections of episode content, based on their locations in the embedding  
709 space. The second criteria was motivated by the observed low off-diagonal values in the episode  
710 trajectory’s temporal correlation matrix (suggesting that the same topic-space coordinates should  
711 not be revisited; see Figure 2A in the main text). For further details on how we created this  
712 low-dimensional embedding space, see *Supporting Information*.

### 713 **Estimating the consistency of flow through topic space across participants**

714 In Figure 6B, we present an analysis aimed at characterizing locations in topic space that dif-  
715 ferent participants move through in a consistent way (via their recall topic trajectories). The  
716 two-dimensional topic space used in our visualizations (Fig. 6) comprised a  $60 \times 60$  (arbitrary  
717 units) square. We tiled this space with a  $50 \times 50$  grid of evenly spaced vertices, and defined a  
718 circular area centered on each vertex whose radius was two times the distance between adjacent  
719 vertices (i.e., 2.4 units). For each vertex, we examined the set of line segments formed by connecting  
720 each pair successively recalled events, across all participants, that passed through this circle. We  
721 computed the distribution of angles formed by those segments and the  $x$ -axis, and used a Rayleigh  
722 test to determine whether the distribution of angles was reliably “peaked” (i.e., consistent across  
723 all transitions that passed through that local portion of topic space). To create Figure 6B we drew

724 an arrow originating from each grid vertex, pointing in the direction of the average angle formed  
725 by the line segments that passed within 2.4 units. We set the arrow lengths to be inversely propor-  
726 tional to the  $p$ -values of the Rayleigh tests at each vertex. Specifically, for each vertex we converted  
727 all of the angles of segments that passed within 2.4 units to unit vectors, and we set the arrow  
728 lengths at each vertex proportional to the length of the (circular) mean vector. We also indicated  
729 any significant results ( $p < 0.05$ , corrected using the Benjamani-Hochberg procedure) by coloring  
730 the arrows in blue (darker blue denotes a lower  $p$ -value, i.e., a longer mean vector); all tests with  
731  $p \geq 0.05$  are displayed in gray and given a lower opacity value.

732 **Searchlight fMRI analyses**

733 In Figure 8, we present two analyses aimed at identifying brain regions whose responses (as partic-  
734 ipants viewed the episode) exhibited a particular temporal structure. We developed a searchlight  
735 analysis wherein we constructed a  $5 \times 5 \times 5$  cube of voxels (following Chen et al., 2017) centered  
736 on each voxel in the brain, and for each of these cubes, computed the temporal correlation matrix  
737 of the voxel responses during episode viewing. Specifically, for each of the 1976 volumes collected  
738 during episode viewing, we correlated the activity patterns in the given cube with the activity  
739 patterns (in the same cube) collected during every other timepoint. This yielded a  $1976 \times 1976$   
740 correlation matrix for each cube. Note: participant 5’s scan ended 75s early, and in Chen et al.,  
741 2017’s publicly released dataset, their scan data was zero-padded to match the length of the other  
742 participants’. For our searchlight analyses, we removed this padded data (i.e., the last 50 TRs),  
743 resulting in a  $1925 \times 1925$  correlation matrix for each cube in participant 5’s brain.

744 Next, we constructed a series of “template” matrices. The first template reflected the timecourse  
745 of the episode’s topic trajectory, and the others reflected the timecourse of each participant’s recall  
746 trajectory. To construct the episode template, we computed the correlations between the topic  
747 proportions estimated for every pair of TRs (prior to segmenting the trajectory into discrete events;  
748 i.e., the correlation matrix shown in Figs. 2B and 8A). We constructed similar temporal correlation  
749 matrices for each participant’s recall topic trajectory (Figs. 2D, S4). However, to correct for length  
750 differences and potential non-linear transformations between viewing time and recall time, we

751 first used dynamic time warping (Berndt and Clifford, 1994) to temporally align participants'  
752 recall topic trajectories with the episode topic trajectory. An example correlation matrix before and  
753 after warping is shown in Fig. 8B. This yielded a  $1976 \times 1976$  correlation matrix for the episode  
754 template and for each participant's recall template.

755 The temporal structure of the episode's content (as described by our model) is captured in the  
756 block-diagonal structure of the episode's temporal correlation matrix (e.g., Figs. 2B, 8A), with time  
757 periods of thematic stability represented as dark blocks of varying sizes. Inspecting the episode  
758 correlation matrix suggests that the episode's semantic content is highly temporally specific (i.e., the  
759 correlations between topic vectors from distant timepoints are almost all near zero). By contrast,  
760 the activity patterns of individual (cubes of) voxels can encode relatively limited information  
761 on their own, and their activity frequently contributes to multiple separate functions (Charron  
762 and Koechlin, 2010; Freedman et al., 2001; Rishel et al., 2013; Sigman and Dehaene, 2008). By  
763 nature, these two attributes give rise to similarities in activity across large timescales that may not  
764 necessarily reflect a single task. To enable a more sensitive analysis of brain regions whose shifts  
765 in activity patterns mirrored shifts in the semantic content of the episode or recalls, we restricted  
766 the temporal correlations we considered to the timescale of semantic information captured by our  
767 model. Specifically, we isolated the upper triangle of the episode correlation matrix and created a  
768 "proximal correlation mask" that included only diagonals from the upper triangle of the episode  
769 correlation matrix up to the first diagonal that contained no positive correlations. Applying this  
770 mask to the full episode correlation matrix was equivalent to excluding diagonals beyond the  
771 corner of the largest diagonal block. In other words, the timescale of temporal correlations we  
772 considered corresponded to the longest period of thematic stability in the episode, and by extension  
773 the longest period of thematic stability in participants' recalls and the longest period of stability we  
774 might expect to see in voxel activity arising from processing or encoding episode content. Figure 8  
775 shows this proximal correlation mask applied to the temporal correlation matrices for the episode,  
776 an example participant's (warped) recall, and an example cube of voxels from our searchlight  
777 analyses.

778 To determine which (cubes of) voxel responses matched the episode template, we correlated

779 the proximal diagonals from the upper triangle of the voxel correlation matrix for each cube with  
780 the proximal diagonals from episode template matrix (Kriegeskorte et al., 2008). This yielded, for  
781 each participant, a voxelwise map of correlation values. We then performed a one-sample *t*-test  
782 on the distribution of (Fisher *z*-transformed) correlations at each voxel, across participants. This  
783 resulted in a value for each voxel (cube), describing how reliably its timecourse followed that of  
784 the episode.

785 We further sought to ensure that our analysis identified regions where the activations' temporal  
786 structure specifically reflected that of the episode, rather than regions whose activity was simply  
787 autocorrelated at a timescale similar to the episode template's diagonal. To achieve this, we used  
788 a phase shift-based permutation procedure, whereby we circularly shifted the episode's topic  
789 trajectory by a random number of timepoints, computed the resulting "null" episode template,  
790 and re-ran the searchlight analysis, in full. (For each of the 100 permutations, the same random shift  
791 was used for all participants). We *z*-scored the observed (unshifted) result at each voxel against  
792 the distribution of permutation-derived "null" results, and estimated a *p*-value by computing  
793 the proportion of shifted results that yielded larger values. To create the map in Figure 8C, we  
794 thresholded out any voxels whose similarity to the unshifted episode's structure fell below the 95<sup>th</sup>  
795 percentile of the permutation-derived similarity results.

796 We used an analogous procedure to identify which voxels' responses reflected the recall tem-  
797 plates. For each participant, we correlated the proximal diagonals from the upper triangle of the  
798 correlation matrix for each cube of voxels with the proximal diagonals from the upper triangle  
799 of their (time-warped) recall correlation matrix. As in the episode template analysis, this yielded  
800 a voxelwise map of correlation coefficients for each participant. However, whereas the episode  
801 analysis compared every participant's responses to the same template, here the recall templates  
802 were unique for each participant. As in the analysis described above, we *t*-scored the (Fisher *z*-  
803 transformed) voxelwise correlations, and used the same permutation procedure we developed for  
804 the episode responses to ensure specificity to the recall timeseries and assign significance values.  
805 To create the map in Figure 8D we again thresholded out any voxels whose scores were below the  
806 95<sup>th</sup> percentile of the permutation-derived null distribution.

807 **Neurosynth decoding analyses**

808 Neurosynth parses a massive online database of over 14,000 neuroimaging studies and constructs  
809 meta-analysis images for over 13,000 psychology- and neuroscience-related terms, based on NIfTI  
810 images accompanying studies where those terms appear at a high frequency. Given a novel image  
811 (tagged with its value type; e.g.,  $t$ -,  $F$ - or  $p$ -statistics), Neurosynth returns a list of terms whose  
812 meta-analysis images are most similar. Our permutation procedure yielded, for each of the two  
813 searchlight analyses, a voxelwise map of  $z$ -values. These maps describe the extent to which each  
814 voxel *specifically* reflected the temporal structure of the episode or individuals' recalls (i.e., relative  
815 to the null distributions of phase-shifted values). We inputted the two statistical maps described  
816 above to Neurosynth to create a list of the 10 most representative terms for each map.

817 **References**

- 818 Atkinson, R. C. and Shiffrin, R. M. (1968). Human memory: A proposed system and its control  
819 processes. In Spence, K. W. and Spence, J. T., editors, *The psychology of learning and motivation*,  
820 volume 2, pages 89–105. Academic Press, New York.
- 821 Baldassano, C., Chen, J., Zadbood, A., Pillow, J. W., Hasson, U., and Norman, K. A. (2017).  
822 Discovering event structure in continuous narrative perception and memory. *Neuron*, 95(3):709–  
823 721.
- 824 Baldassano, C., Hasson, U., and Norman, K. A. (2018). Representation of real-world event schemas  
825 during narrative perception. *Journal of Neuroscience*, 38(45):9689–9699.
- 826 Berndt, D. J. and Clifford, J. (1994). Using dynamic time warping to find patterns in time series. In  
827 *KDD workshop*, volume 10, pages 359–370.
- 828 Blei, D. M. and Lafferty, J. D. (2006). Dynamic topic models. In *Proceedings of the 23rd International  
829 Conference on Machine Learning*, ICML '06, pages 113–120, New York, NY, US. ACM.

- 830 Blei, D. M., Ng, A. Y., and Jordan, M. I. (2003). Latent dirichlet allocation. *Journal of Machine*  
831 *Learning Research*, 3:993 – 1022.
- 832 Brown, T. B., Mann, B., Ryder, N., Subbiah, M., Kaplan, J., Dhariwal, P., Neelakantan, A., Shyam,  
833 P., Sastry, G., Askell, A., Agarwal, S., Herbert-Voss, A., Krueger, G., Henighan, T., Child, R.,  
834 Ramesh, A., Ziegler, D. M., Wu, J., Winter, C., Hesse, C., Chen, M., Sigler, E., Litwin, M., Gray, S.,  
835 Chess, B., Clark, J., Berner, C., McCandlish, S., Radford, A., Sutskever, I., and Amodei, D. (2020).  
836 Language models are few-shot learners. *arXiv*, 2005.14165.
- 837 Brunec, I. K., Moscovitch, M. M., and Barense, M. D. (2018). Boundaries shape cognitive represen-  
838 tations of spaces and events. *Trends in Cognitive Sciences*, 22(7):637–650.
- 839 Capota, M., Turek, J., Chen, P.-H., Zhu, X., Manning, J. R., Sundaram, N., Keller, B., Wang, Y., and  
840 Shin, Y. S. (2017). Brain imaging analysis kit.
- 841 Cer, D., Yang, Y., Kong, S. Y., Hua, N., Limtiaco, N., John, R. S., Constant, N., Guajardo-Cespedes,  
842 M., Yuan, S., Tar, C., Sung, Y.-H., Strope, B., and Kurzweil, R. (2018). Universal sentence encoder.  
843 *arXiv*, 1803.11175.
- 844 Charron, S. and Koechlin, E. (2010). Divided representations of current goals in the human frontal  
845 lobes. *Science*, 328(5976):360–363.
- 846 Chen, J., Leong, Y. C., Honey, C. J., Yong, C. H., Norman, K. A., and Hasson, U. (2017). Shared  
847 memories reveal shared structure in neural activity across individuals. *Nature Neuroscience*,  
848 20(1):115.
- 849 Clewett, D. and Davachi, L. (2017). The ebb and flow of experience determines the temporal  
850 structure of memory. *Curr Opin Behav Sci*, 17:186–193.
- 851 Dobrushin, R. L. (1970). Prescribing a system of random variables by conditional distributions.  
852 *Theory of Probability & Its Applications*, 15(3):458–486.
- 853 DuBrow, S. and Davachi, L. (2013). The influence of contextual boundaries on memory for the  
854 sequential order of events. *Journal of Experimental Psychology: General*, 142(4):1277–1286.

- 855 Ezzyat, Y. and Davachi, L. (2011). What constitutes an episode in episodic memory? *Psychological*  
856 *Science*, 22(2):243–252.
- 857 Fisher, R. A. (1925). *Statistical Methods for Research Workers*. Oliver and Boyd.
- 858 Freedman, D., Riesenhuber, M., Poggio, T., and Miller, E. (2001). Categorical representation of  
859 visual stimuli in the primate prefrontal cortex. *Science*, 291(5502):312–316.
- 860 Hasson, U., Chen, J., and Honey, C. J. (2015). Hierarchical process memory: memory as an integral  
861 component of information processing. *Trends in Cognitive Science*, 19(6):304–315.
- 862 Hasson, U., Yang, E., Vallines, I., Heeger, D. J., and Rubin, N. (2008). A hierarchy of temporal  
863 receptive windows in human cortex. *Journal of Neuroscience*, 28(10):2539–2550.
- 864 Heusser, A. C., Ezzyat, Y., Shiff, I., and Davachi, L. (2018a). Perceptual boundaries cause mnemonic  
865 trade-offs between local boundary processing and across-trial associative binding. *Journal of*  
866 *Experimental Psychology Learning, Memory, and Cognition*, 44(7):1075–1090.
- 867 Heusser, A. C., Fitzpatrick, P. C., Field, C. E., Ziman, K., and Manning, J. R. (2017). Quail: a  
868 Python toolbox for analyzing and plotting free recall data. *The Journal of Open Source Software*,  
869 10.21105/joss.00424.
- 870 Heusser, A. C., Ziman, K., Owen, L. L. W., and Manning, J. R. (2018b). HyperTools: a Python  
871 toolbox for gaining geometric insights into high-dimensional data. *Journal of Machine Learning*  
872 *Research*, 18(152):1–6.
- 873 Howard, M. W. and Kahana, M. J. (2002). A distributed representation of temporal context. *Journal*  
874 *of Mathematical Psychology*, 46:269–299.
- 875 Howard, M. W., MacDonald, C. J., Tiganj, Z., Shankar, K. H., Du, Q., Hasselmo, M. E., and H., E.  
876 (2014). A unified mathematical framework for coding time, space, and sequences in the medial  
877 temporal lobe. *Journal of Neuroscience*, 34(13):4692–4707.
- 878 Howard, M. W., Viskontas, I. V., Shankar, K. H., and Fried, I. (2012). Ensembles of human MTL  
879 neurons “jump back in time” in response to a repeated stimulus. *Hippocampus*, 22:1833–1847.

- 880 Huk, A., Bonnen, K., and He, B. J. (2018). Beyond trial-based paradigms: continuous behavior, on-  
881 going neural activity, and naturalistic stimuli. *Journal of Neuroscience*, 10.1523/JNEUROSCI.1920-  
882 17.2018.
- 883 Huth, A. G., de Heer, W. A., Griffiths, T. L., Theunissen, F. E., and Gallant, J. L. (2016). Natural  
884 speech reveals the semantic maps that tile human cerebral cortex. *Nature*, 532:453–458.
- 885 Huth, A. G., Nisimoto, S., Vu, A. T., and Gallant, J. L. (2012). A continuous semantic space describes  
886 the representation of thousands of object and action categories across the human brain. *Neuron*,  
887 76(6):1210–1224.
- 888 Kahana, M. J. (1996). Associative retrieval processes in free recall. *Memory & Cognition*, 24:103–109.
- 889 Kahana, M. J. (2012). *Foundations of Human Memory*. Oxford University Press, New York, NY.
- 890 Koriat, A. and Goldsmith, M. (1994). Memory in naturalistic and laboratory contexts: distin-  
891 guishing accuracy-oriented and quantity-oriented approaches to memory assessment. *Journal of*  
892 *Experimental Psychology: General*, 123(3):297–315.
- 893 Kriegeskorte, N., Mur, M., and Bandettini, P. (2008). Representational similarity analysis – con-  
894 nnecting the branches of systems neuroscience. *Frontiers in Systems Neuroscience*, 2:1 – 28.
- 895 Landauer, T. K. and Dumais, S. T. (1997). A solution to Plato’s problem: the latent semantic  
896 analysis theory of acquisition, induction, and representation of knowledge. *Psychological Review*,  
897 104:211–240.
- 898 Lerner, Y., Honey, C. J., Silbert, L. J., and Hasson, U. (2011). Topographic mapping of a hierarchy  
899 of temporal receptive windows using a narrated story. *Journal of Neuroscience*, 31(8):2906–2915.
- 900 Manning, J. R. (2019). Episodic memory: mental time travel or a quantum ‘memory wave’ function?  
901 *PsyArXiv*, doi:10.31234/osf.io/6zjwb.
- 902 Manning, J. R. (2020). Context reinstatement. In Kahana, M. J. and Wagner, A. D., editors, *Handbook*  
903 *of Human Memory*. Oxford University Press.

- 904 Manning, J. R., Norman, K. A., and Kahana, M. J. (2015). The role of context in episodic memory.  
905 In Gazzaniga, M., editor, *The Cognitive Neurosciences, Fifth edition*, pages 557–566. MIT Press.
- 906 Manning, J. R., Polyn, S. M., Baltuch, G., Litt, B., and Kahana, M. J. (2011). Oscillatory patterns  
907 in temporal lobe reveal context reinstatement during memory search. *Proceedings of the National  
908 Academy of Sciences, USA*, 108(31):12893–12897.
- 909 McInnes, L., Healy, J., and Melville, J. (2018). UMAP: Uniform manifold approximation and  
910 projection for dimension reduction. *arXiv*, 1802(03426).
- 911 Mikolov, T., Chen, K., Corrado, G., and Dean, J. (2013). Efficient estimation of word representations  
912 in vector space. *arXiv*, 1301.3781.
- 913 Mueller, A., Fillion-Robin, J.-C., Boidol, R., Tian, F., Nechifor, P., yoonsubKim, Peter, Rampin, R.,  
914 Corvellec, M., Medina, J., Dai, Y., Petrushev, B., Langner, K. M., Hong, Alessio, Ozsváld, I.,  
915 vkolmakov, Jones, T., Bailey, E., Rho, V., IgorAPM, Roy, D., May, C., foobuzz, Piyush, Seong,  
916 L. K., Goey, J. V., Smith, J. S., Gus, and Mai, F. (2018). WordCloud 1.5.0: a little word cloud  
917 generator in Python. *Zenodo*, <https://zenodo.org/record/1322068#.W4tPKZNKh24>.
- 918 Murdock, B. B. (1962). The serial position effect of free recall. *Journal of Experimental Psychology*,  
919 64:482–488.
- 920 Paller, K. A. and Wagner, A. D. (2002). Observing the transformation of experience into memory.  
921 *Trends in Cognitive Sciences*, 6(2):93–102.
- 922 Pedregosa, F., Varoquaux, G., Gramfort, A., Michel, V., Thirion, B., Grisel, O., Blondel, M., Pretten-  
923 hofer, P., Weiss, R., Dubourg, V., Vanderplas, J., Passos, A., Cournapeau, D., Brucher, M., Perrot,  
924 M., and Duchesnay, E. (2011). Scikit-learn: Machine learning in Python. *Journal of Machine  
925 Learning Research*, 12:2825–2830.
- 926 Polyn, S. M., Norman, K. A., and Kahana, M. J. (2009). A context maintenance and retrieval model  
927 of organizational processes in free recall. *Psychological Review*, 116(1):129–156.

- 928 Postman, L. and Phillips, L. W. (1965). Short-term temporal changes in free recall. *Quarterly Journal*  
929      *of Experimental Psychology*, 17:132–138.
- 930 Rabiner, L. (1989). A tutorial on Hidden Markov Models and selected applications in speech  
931      recognition. *Proceedings of the IEEE*, 77(2):257–286.
- 932 Radford, A., Wu, J., Child, R., Luan, D., Amodei, D., and Sutskever, I. (2019). Language models are  
933      unsupervised multitask learners. *OpenAI Blog*, 1(8).
- 934 Radvansky, G. A. and Zacks, J. M. (2017). Event boundaries in memory and cognition. *Curr Opin*  
935      *Behav Sci*, 17:133–140.
- 936 Ramdas, A., Trillos, N., and Cuturi, M. (2017). On wasserstein two-sample testing and related  
937      families of nonparametric tests. *Entropy*, 19(2):47.
- 938 Ranganath, C. and Ritchey, M. (2012). Two cortical systems for memory-guided behavior. *Nature*  
939      *Reviews Neuroscience*, 13:713 – 726.
- 940 Rishel, C. A., Huang, G., and Freedman, D. J. (2013). Independent category and spatial encoding  
941      in parietal cortex. *Neuron*, 77(5):969–979.
- 942 Sigman, M. and Dehaene, S. (2008). Brain mechanisms of serial and parallel processing during  
943      dual-task performance. *Journal of Neuroscience*, 28(30):7585–7589.
- 944 Simony, E. and Chang, C. (2020). Analysis of stimulus-induced brain dynamics during naturalistic  
945      paradigms. *NeuroImage*, 216:116461.
- 946 Simony, E., Honey, C. J., Chen, J., and Hasson, U. (2016). Uncovering stimulus-locked network  
947      dynamics during narrative comprehension. *Nature Communications*, 7(12141):1–13.
- 948 Tompry, A. and Davachi, L. (2017). Consolidation promotes the emergence of representational  
949      overlap in the hippocampus and medial prefrontal cortex. *Neuron*, 96(1):228–241.
- 950 Welch, G. B. and Burnett, C. T. (1924). Is primacy a factor in association-formation. *American Journal*  
951      *of Psychology*, 35:396–401.

- 952 Yarkoni, T., Poldrack, R. A., Nichols, T. E., Van Essen, D. C., and Wager, T. D. (2011). Large-scale  
953 automated synthesis of human functional neuroimaging data. *Nature Methods*, 8(8):665.
- 954 Yonelinas, A. P. (2002). The nature of recollection and familiarity: A review of 30 years of research.  
955 *Journal of Memory and Language*, 46:441–517.
- 956 Zacks, J. M., Speer, N. K., Swallow, K. M., Braver, T. S., and Reynolds, J. R. (2007). Event perception:  
957 a mind-brain perspective. *Psychological Bulletin*, 133:273–293.
- 958 Zadbood, A., Chen, J., Leong, Y. C., Norman, K. A., and Hasson, U. (2017). How we transmit  
959 memories to other brains: Constructing shared neural representations via communication. *Cereb*  
960 *Cortex*, 27(10):4988–5000.
- 961 Zwaan, R. A. and Radvansky, G. A. (1998). Situation models in language comprehension and  
962 memory. *Psychological Bulletin*, 123(2):162 – 185.

## 963 Supporting information

964 Supporting information is available in the online version of the paper.

## 965 Acknowledgements

966 We thank Luke Chang, Janice Chen, Chris Honey, Lucy Owen, Emily Whitaker, and Kirsten Ziman  
967 for feedback and scientific discussions. We also thank Janice Chen, Yuan Chang Leong, Kenneth  
968 Norman, and Uri Hasson for sharing the data used in our study. Our work was supported in part  
969 by NSF EPSCoR Award Number 1632738. The content is solely the responsibility of the authors  
970 and does not necessarily represent the official views of our supporting organizations.

971 **Author contributions**

972 Conceptualization: A.C.H. and J.R.M.; Methodology: A.C.H., P.C.F. and J.R.M.; Software: A.C.H.,  
973 P.C.F. and J.R.M.; Analysis: A.C.H., P.C.F. and J.R.M.; Writing, Reviewing, and Editing: A.C.H.,  
974 P.C.F. and J.R.M.; Supervision: J.R.M.

975 **Author information**

976 The authors declare no competing financial interests. Correspondence and requests for materials  
977 should be addressed to J.R.M. (jeremy.r.manning@dartmouth.edu).